Available online at www.sciencedirect.com

ScienceDirect

Energy Procedia 8 (2011) 167–173

Energy Procedia

Silicon PV – 1st International Conference on Silicon Photovoltaics

Solar cell emitter design with PV-tailored implantation

T. Ohrdes[a]*, S. Steingrube[b], H. Wagner[b], C. Zechner[c], G. Letay[c], R. Chen[d], S. T. Dunham[d], P. P. Altermatt[b]

[a] *Institute for Solar Energy Research Hamelin (ISFH), Am Ohrberg 1, 31860 Emmerthal, Germany*
[b] *Leibniz University of Hannover, Institute for Solid State Physics, Dep. Solar Energy, Appelstr. 2, 30167 Hannover, Germany*
[c] *SYNOPSYS Switzerland LLC, Thurgauerstrasse 40, Zurich, Switzerland*
[d] *Department of Electrical Engineering, University of Washington, Seattle, WA 98195, USA*

Abstract

A potentially cost-effective ion implanter for solar cells has become commercially available very recently. As the emitter dopant profiles differ from the standard diffusions, a combination of process simulation and device simulation is used to predict possible applications as front emitter. The simulations show that ion energies of 10 to 30 keV and doses in the range of 5×10^{14} to 7×10^{15} cm^{-2} are sufficient for reducing the phosphorus peak density and, hence, obtaining cell efficiency levels above 20%, if appropriate surface passivation and wafer materials are used. The simulations strongly indicate, however, that cell efficiency improves only marginally if the cell has a fully metallized rear Al-BSF and a boron-doped Cz base in the degraded state. Simulated cells with a local rear Al-BSF show an efficiency improvement of more than 0.3% absolute in the degraded state.

© 2011 Published by Elsevier Ltd. Open access under CC BY-NC-ND license.
Selection and/or peer-review under responsibility of SiliconPV 2011

Keywords: device simulation; process simulation; Si solar cells; implantation

* Corresponding author. ohrdes@isfh.de.

1876–6102 © 2011 Published by Elsevier Ltd. Selection and/or peer-review under responsibility of SiliconPV 2011.
Open access under CC BY-NC-ND license. doi:10.1016/j.egypro.2011.06.119

1. Introduction

An ion implanter has become commercially available specifically tailored to solar cells [1]. For forming emitters, rather low ion doses are necessary, which require such a short time for implantation that the mechanical handling of the wafers limits the throughput. Selective emitters can be implanted with masks. Costs may be saved because there is no edge isolation necessary, and the removal of a phosphosilicate glass layer is not required. A passivating oxide can be grown during annealing.

In contrast to the IC industry, the excess carrier lifetimes are important in PV. Therefore, rapid thermal anneal (RTA), usually applied in the IC industry, is not feasible [2]. Instead, a furnace anneal is necessary with a thermal budget similar to the standard phosphorus diffusion. We model favorable conditions by a combination of implantation, annealing, and device simulations.

2. Implantation models

Emitter formation by ion implantation and subsequent thermal annealing offers a flexible emitter design. By selecting the implant energy and dose, one can determine the distribution of P atoms after implantation. During ion implantation, the surface region of the silicon wafer gets amorphized. This region recrystallizes by solid phase epitaxial regrowth (SPER) at the onset of thermal annealing. In the deeper non-amorphized regions, the implantation process creates a high concentration of point defects: silicon self interstitials (I) and vacancies (V). During thermal annealing, these point defects can recombine or diffuse to the surface or form larger clusters of defects, such as {311} defects or dislocation loops [3]. After sufficiently long diffusion time, these clusters dissolve again into point defects, which diffuse towards the wafer surface and recombine. Until all defects are dissolved, the concentration of I is above thermal equilibrium, and the P diffusion via P-I pairs is enhanced. For an overview on diffusion mechanisms in silicon, see for example [4,5]. For solar cell emitter formation, phosphorus ions are implanted into the Si wafer with energies in the range of 10's of keV. The generated crystal defects can be annealed at furnace temperatures typical for solar cell phosphorus diffusion.

For process modeling, it is necessary to account for (i) the spatial distribution of dopant atoms and point defects after implantation, (ii) amorphization of Si, (iii) formation and dissolution of crystal defects during the annealing, and (iv) I and V mediated dopant diffusion. We use the process simulator SENTAURUS PROCESS [6], which is widely used in IC industry, together with its standard models. As an illustration of the model accuracy, Fig. 1(a) compares our simulation result of a P emitter profile to SIMS data from Benick et al. [2].

Figure 1(b) shows simulation results of various phosphorus profiles. The higher dose of 7×10^{15} cm^{-2} is used for regions under the metal contacts, which require a high surface concentration of P. The device simulation below in Sec. 3 yields very similar cell efficiencies independently of annealing time in the range between 20 and 40 minutes at 890ºC. It is apparent that both a low surface density and a deep metallurgical junction depth can be attained with implantation. It was predicted already in Ref. [7] that such emitters have the lowest saturation currents J_0 if an effective surface passivation can be achieved. Fig. 1(c) shows two improved homogeneous emitter designs achieved by standard $POCl_3$ diffusions [8]. The homogeneous oxidized emitter will be used for comparison with the implanted, selective emitter below.

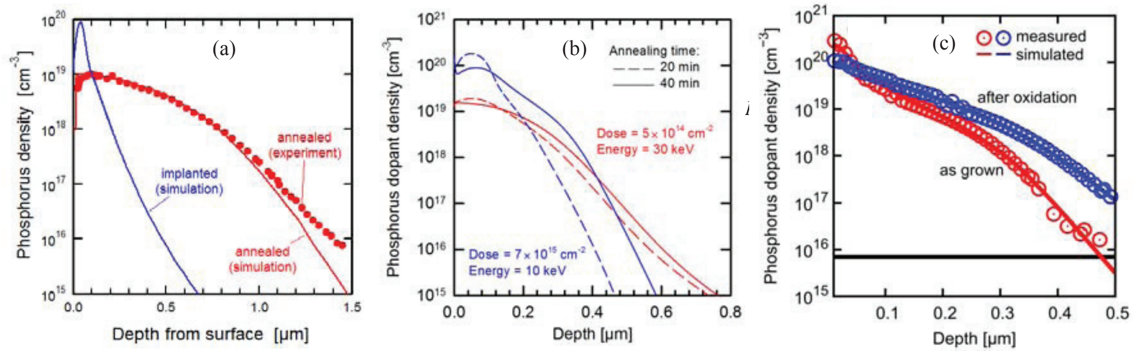

Fig. 1. (a): Experimental phosphorus profile after implantation and annealing from Benick et al. [2] (symbols) and our simulation (lines). (b): Our simulated phosphorus emitter profiles. (c): $POCl_3$ profiles from Ref. [8], ECV measurements and simulations [9].

Table 1. A set of device simulation models and parameters that has been developed specifically for the simulation of Si solar cells.

Device simulation	
Equations numerically solved	Semiconductor drift-diffusion equations
Temperature	300 K
Free carrier statistics	Fermi-Dirac
Intrinsic carrier density	$n_i = 9.65 \times 10^9$ cm^{-3} [10]
	Obtained with setting E_g to a lower value in [11]
Band gap narrowing model	Schenk [12]
Free carrier mobility	Klaassen's unified mobility model [13,14]
Radiative recombination	$B = 4.73 \times 10^{-15}$ cm^3/s [15]
Its doping and injection-dependence	See [16] and [17]
Auger recombination	Dziewior and Schmid [18]
Its temperature dependence [19]	$C_{(n,p)} = (A + B(T/T_0) + C(T/T_0)^2)(1+He^{-(n,p)/N0})$
	$A = 2.8 \times 10^{-31}$, 7.91×10^{-32} cm^6/s; $B = 0$, -1.239×10^{-32} cm^6/s
	$C = 0$, 3.231×10^{-32} cm^6/s; $H = 8, 8$
	$N_0 = 2.5 \times 10^{17}$ cm^{-3}, $N_0 = 2.5 \times 10^{17}$ cm^{-3}; $T_0 = 300$K
SRH bulk recombination	Boron-doped Cz silicon: Refs. [20,21,22]
	Undegraded state: equal lifetime parameters, midgap
SRH surface recombination	Phosphorus-diffused surfaces: Ref. [23]
Optical simulation	
Solar spectrum	Standard AM1.5g, i.e. calculated with SMARTS [24]
Optical dispersion relations	Silicon from Green [25], Al from Shiles [26]
	SiN_x measured at ISFH.

3. Device simulation

For our two-dimensional numerical device simulations [27], we use the device simulator SENTAURUS DEVICE [6], which is widely used in the IC and PV industry, with the device models listed in Table 1.

4. Results

Generally, implantation of the emitter leads to efficiency improvements only if the recombination losses in the remaining device parts are similar or lower than the losses in the emitter. To assess the

benefits, we use as a reference the simulations of two experimentally fabricated cell structures of Ref. [9]: one cell structure is a standard industrial design but with a $POCl_3$ emitter that has been oxidized for 15 minutes at 900ºC, the other structure has the same emitter but the rear is contacted by Al-BSF fingers instead of being fully metalized. The emitter and the non-metallized parts of the rear are passivated with a SiO_2/SiN_x stack. In our simulations, we replace the front $POCl_3$ emitter with an implanted selective emitter, but keep the same SiO_2/SiN_x stack as passivation layer. The resulting I-V parameters are shown in Fig. 2.

It is apparent that the I-V parameters of a fully metalized Al-BSF cell do only marginally benefit from an implanted emitter. The recombination losses in the Al-BSF are rather high [9] and start dominating the total losses when the emitter is significantly improved. This is obtained assuming a non-degraded 2.5 Ωcm boron-doped Cz base with a SRH lifetime of 280 µs. After degradation, the benefits from an implanted emitter are further reduced because the recombination losses in the base dominate.

In contrast, the cell with the local Al-BSF shows an efficiency improvement by more than 0.3% absolute with implanting. This is due to an improvement in V_{oc} and to some extent in J_{sc}, despite the reduction in FF due to the local rear contacts (the rear contact pattern and the corresponding base resistivity are not fully optimized). Again, a SRH lifetime of 280 µs is assumed. Degradation has a far larger impact on the I-V parameters compared to a cell with a fully metalized rear, for the following reasons. Degradation causes the SRH lifetime in the boron-doped Cz base to be strongly injection dependent. The lifetime improves considerably going from MPP to the open-circuit condition, and thus causes a low fill factor. See Ref. [9] for more details.

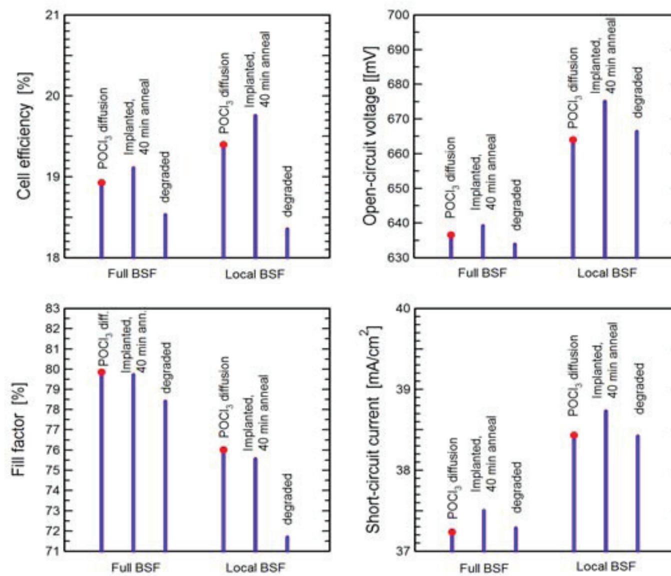

Fig. 2. Simulated I-V parameters. The reference cells with a $POCl_3$ diffusion, shown in Fig. 1(c), is a reproduction of an experiment from [9] shown here as red dots. The adjacent bars indicate a simulation with the implanted emitter of Fig. 1(b) before and after degradation of the 2.5 Ωcm boron-doped Cz base with an interstitial oxygen density of 7×10^{17} cm^{-3} [20].

Crucial for the benefits of an implanted emitter is an effective front surface passivation. By comparing fabricated with simulated cells, we found that the recombination velocity parameter S_p of our SiO_2/SiN_x stacks at the front surface can be approximately parameterized as

$$S_p[\text{cm/s}] = 500(N_{don}/10^{19}\ \text{cm}^{-3})^{0.6} + 60\ (N_{don}/10^{19}\ \text{cm}^{-3})^3 \quad (1)$$

This parameterization is similar to an alnealed oxide in Ref. [23], probably because both the Al layer and the SiN_x layer release similar amounts of hydrogen into the oxide during the firing step. Fig. 3 shows the influence of the surface passivation of the cell with the local BSF in the non-degraded state. A rather small reduction in efficiency is predicted for a tenfold increase in the SRH parameter S_p, but even higher S_p values reduce cell efficiency considerably.

Finally, Fig. 4 depicts the I-V parameters as a function of the implanted dose. While a low dose creates an emitter with low recombination but high resistive losses, a high dose does results in the opposite, and hence an optimum dose exists. The profiles shown in Fig. 1(b) have a sheet resistivity of 165 Ω/sq or 50 Ω/sq, respectively. The optimum depends on the specific passivation quality and the specific front metallization (e.g. finger distance and finger width) and should be simulated for each cell manufacturer individually.

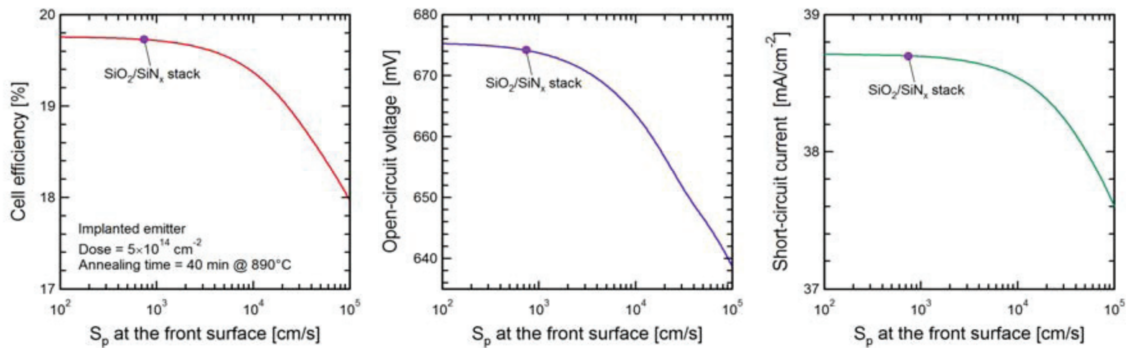

Fig. 3. Simulated I-V parameters as a function of the SRH parameter S_p at the emitter surface.

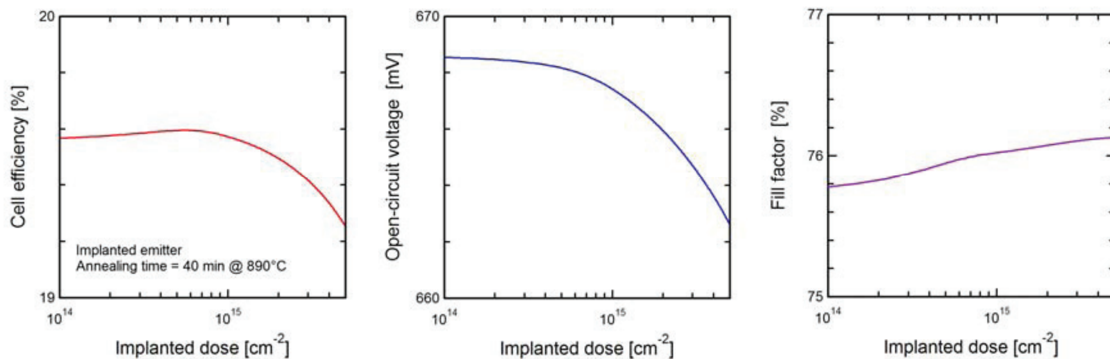

Fig. 4. Simulated I-V parameters as a function of the implanted dose. With increasing dose, there are decreasing resistive losses and increasing recombination losses. The optimum depends on the front metallization geometry and the front surface passivation.

5. Conclusions

Simulations show that phosphorus ion energies of 10 – 30 keV and implantation doses near 5×10^{14} cm^{-2} for the emitter between the fingers and doses of 7×10^{15} cm^{-2} under the front metal fingers are suitable for reducing the phosphorus peak density at the surface. Cell efficiency levels above 20% can only be achieved if appropriate surface passivation and wafer materials are used. The simulations strongly indicate that cell efficiency improves only marginally if the cell has a fully metallized rear Al-BSF and a boron-doped Cz base in a degraded state. Simulated cells with a local rear Al-BSF show an efficiency improvement due to an implanted selective emitter design by more than 0.3% absolute.

References

[1] Varian, Gloucester, MA.

[2] Benick J, Bateman N, Hermle M. Very low saturation current densities on ion implanted boron emitters. *25th EU PV Solar Energy Conf.* Valencia, Spain, 2010, p. 1169.

[3] Cristiano F et al. Thermal Evolution of Extrinsic Defects in Ion Implanted Silicon: Current Understanding and Modelling. Mat. Res. Soc. Symp. Proc. 717. *Silicon Front-End Junction Formation Technologies*. 2002;C5.7.1–C5.7.12.

[4] Plummer JD, Deal MD, Griffin PB. *Silicon VLSI technology*. New York: Prentice Hall; 2000.

[5] Pichler P. *Intrinsic Point Defects, Impurities and Their Diffusion in Silicon*. Venna: Springer; 2004.

[6] Sentaurus Process User Guide, Version E-2010.12, Synopsys, Inc., Mountain View, CA

[7] Cuevas A, Balbuena M. Thick-emitter silicon solar cells. *20th IEEE Specialists Conf.*, Las Vegas, 1988, p.429

[8] S. Gatz, H. Hannebauer, R. Hesse, F. Werner, A. Schmidt1, T. Dullweber, J. Schmidt, K. Bothe, R. Brendel. 19.4%-efficient large-area fully screen-printed silicon solar cells. *Phys. Status Solidi RRL* 2011;**5**:147.

[9] See the contribution from S. Steingrube et al. at this conference.

[10] Altermatt PP, Schenk A, Geelhaar G, Heiser G. Reassessment of the intrinsic carrier density in crystalline silicon in view of band-gap narrowing. *Journal of Applied Physics* 2003;**93**:1598.

[11] Green MA. Intrinsic Concentration, Effective Densities of States, and Effective Mass in Silicon. *Journal of Applied Physics* 1990;**67**:2944.

[12] Schenk A. Finite-temperature full random-phase approximation model of band gap narrowing for silicon device simulation. *Journal of Applied Physics* 1998;**84**:3684.

[13] Klaassen DBM. A Unified Mobility Model for Device Simulation – I. Model Equations and Concentration Dependence. *Solid-State Electronics* 1992;**35**:953.

[14] Klaassen DBM. A Unified Mobility Model for Device Simulation – II. Temperature Dependence of Carrier Mobility and Lifetime. *Solid-State Electronics* 1992;**35**:961.

[15] Trupke T, Green MA, Würfel P, Altermatt PP, Wang A, Zhao J, Corkish R. Temperature dependence of the radiative recombination coefficient of intrinsic crystalline silicon. *Journal of Applied Physics* 2003;**94**:4930.

[16] Altermatt PP, Geelhaar F, Trupke T, Day X, Neisser A, Daub E. Injection dependence of spontaneous radiative recombination in c-Si: experiment, theoretical analysis, and simulation. *Proc. 5th International Conference on Numerical Simulation of Optoelectronic Devices (NUSOD05)*, IEEE, NY, 2005, p. 47.

[17] Altermatt PP, Geelhaar F, Trupke T, Dai X, Neisser A, Daub E. Injection dependence of spontaneous radiative recombination in crystalline silicon: Experimental verification and theoretical analysis. *Applied Physics Letters* 2006;**88**:261901.

[18] Dziewior J, Schmid W. Auger coefficients for highly doped and highly excited silicon. *Applied Physics Letters* 1977;**31**:346.

[19] Altermatt PP, Schmidt J, Heiser G, Aberle AG. Assessment and Parameterisation of Coulomb-Enhanced Auger Recombination Coefficients in Lowly Injected Crystalline Silicon. *Journal of Applied Physics* 1997;**82**:4938.

[20] Bothe K, Sinton R, Schmidt J. Fundamental Boron-Oxygen-related Carrier Lifetime Limit in Mono- and Multicrystalline Silicon. *Progress in PV* 2005;**13**:287.

[21] Schmidt J,Cuevas A. Electronic properties of light-induced recombination centers in boron-doped Czochralski silicon. *Journal of Applied Physics* 1999;**86**;3175.

[22] Rein S, Glunz SW. Electronic properties of the metastable defect in boron-doped Czochralski silicon: Unambiguous determination by advanced lifetime spectroscopy. *Journal of Applied Physics* 2003;**82**:1054.

[23] Altermatt PP, Schumacher JO, Cuevas A, Kerr MJ, Glunz SW, King RR, Heiser G.Numerical modeling of highly doped Si:P emitters based on Fermi–Dirac statistics and self-consistent material parameters. *Journal of Applied Physics* 2002;**92**:3187.

[24] Gueymard C. Parameterized Transmittance Model for Direct Beam and Circumsolar Spectral Irradiance. *Solar Energy* 2001;**71**:325.

[25] Green MA. Self-consistent optical parameters of intrinsic silicon at 300 K including temperature coefficients. *Solar Energy Materials and Solar Cells* 2008;**92**:1305.

[26] Shiles E, Sasaki T, Inokuti M, Smith DY. Self-consistency and sum-rule tests in the Kramers-Kronig analysis of optical data: Application to aluminium. *Physical Review B* 1980:**22**:1612.

[27] Altermatt PP, Dreissigacker S, Yang Y, Sprodowski C, Dezhdar T, Koc S, Veith B, Herrman S, Bock R, Bothe K, Schmidt J, Brendel R. Highly predictive modelling of entire Si solar cells for industrial applications. 24th European PV Solar Energy Conference, Hamburg, Germany, (WIP, Munich), 2009, p. 901